We are IntechOpen, the world's leading publisher of Open Access books Built by scientists, for scientists

4,800
Open access books available

122,000
International authors and editors

135M
Downloads

Our authors are among the

154
Countries delivered to

TOP 1%
most cited scientists

12.2%
Contributors from top 500 universities

CLARIVATE ANALYTICS BOOK CITATION INDEX INDEXED

WEB OF SCIENCE™

Selection of our books indexed in the Book Citation Index in Web of Science™ Core Collection (BKCI)

Interested in publishing with us?
Contact book.department@intechopen.com

Numbers displayed above are based on latest data collected.
For more information visit www.intechopen.com

1

Optical Turbulence Profiles in the Atmosphere

Remy Avila
Centro de Física Aplicada y Tecnología Avanzada,
Universidad Nacional Autónoma de México
Centro de Radioastronomía y Astrofísica,
Universidad Nacional Autónoma de México
México

1. Introduction

Turbulence induces phase fluctuations on light waves traveling through the atmosphere. The main effect of those perturbations on imaging systems is to diminish the attainable angular resolution, whereas on free-space laser communications the turbulence drastically affects system performances. Adaptive Optical (AO) methods are aimed at reducing those cumbersome effects by correcting the phase disturbances introduced by atmospheric turbulence. The development of such methods would not have seen the light without research of the turbulent fluctuations of the refractive index of air, the so called Optical Turbulence (OT). It is necessary to study the statistical properties of the perturbed wavefront to design specific AO systems and to optimize their performances. Some of the useful parameters for this characterization and their impact on AO are the following: The Fried parameter r_0 (Fried, 1966), which is inversely proportional to the width of the image of point-like source (called "seeing"), leads to the determination of the spatial sampling of the wavefront for a given degree of correction (Rousset, 1994). r_0 is the dominant parameter in the calculation of the phase fluctuation variance. The coherence time τ_0 (Roddier, 1999), during which the wavefront remains practically unchanged, is needed to determine the temporal bandwidth of an AO system and the required brightness of the reference sources used to measure the wavefront. The isoplanatic angle θ_0 (Fried, 1982), corresponding to the field of view over which the wavefront perturbations are correlated, determines the angular distance between the corrected and the reference objects, for a given degree of correction.

The parameters described in the last paragraph depend on the turbulence conditions encountered by light waves along its travel through the atmosphere. The principal physical quantities involved are the vertical profile of the refractive index structure constant $C_N^2(h)$, which indicates the optical turbulence intensity, and the vertical profile of the wind velocity $\mathbf{V}(h)$, where h is the altitude above the ground.

The profiles $C_N^2(h)$ and $\mathbf{V}(h)$ can be measured with balloons equipped with thermal micro sensors and a GPS receiver. This method enables detailed studies of optical turbulence and its physical causes but it is not well suited to follow the temporal evolution of the measured parameters along the night nor to gather large enough data series to perform statistical studies. To do so, it is convenient to use remote sensing techniques like Scintillation Detection and Ranging (SCIDAR) (Rocca et al., 1974) and its modern derivatives like Generalized

SCIDAR (Avila et al., 1997; Fuchs et al., 1998) and Low Layer SCIDAR (Avila et al., 2008). Those techniques make use of statistical analysis of double star scintillation images recorded either on the telescope pupil plane (for the classical SCIDAR) or on a virtual plane located a few kilometers below the pupil. Because of this difference, the classical SCIDAR is insensitive to turbulence within the first kilometer above the ground. The Generalized SCIDAR can measure optical turbulence along the whole path in the atmosphere but with an altitude resolution limited to 500 m on 1 to 2-m-class telescopes and the Low Layer SCIDAR can achieve altitude sampling as thin as 8 m but only within the first 500 m using a portable 40-cm telescope. Another successful remote optical-turbulence profiler that has been developed and largely deployed in the last decade is the Slope Detection and Ranging (SLODAR) which uses statistical analysis of wavefront-slope maps measured on double stars (Butterley et al., 2006; Wilson et al., 2008; Wilson et al., 2004). In this book chapter, only SCIDAR related techniques and results are presented.

In § 2 I introduce the main concepts of atmospheric optical turbulence, including some effects on the propagation of optical waves and image formation.The Generalized SCIDAR and Low Layer SCIDAR techniques are explained in § 3. § 4 is devoted to showing some examples of results obtained by monitoring optical turbulence profiles with the afore-mentioned techniques. Finally a summary of the chapter is put forward in § 5.

2. Atmospheric optical turbulence

2.1 Kolmogorov turbulence

The turbulent flow of a fluid is a phenomenon widely spread in nature. In his book "La turbulence", Lesieur (1994) gives a large number of examples where turbulence is found. The air circulation in the lungs as well as gas movement in the interstellar medium are turbulent flows. A spectacular example of turbulence is shown in Fig. 1 where an image of a zone of Jupiter's atmosphere is represented.

Since Navier's work in the early 19th century, the laws governing the movement of a fluid are known. They are expressed in the form of the Navier-Stokes equations. For the case of a turbulent flow, those equations are still valid and contain perhaps all the information about turbulence. However, the stronger the turbulence, the more limited in time and space are the solutions of those differential equations. This non-deterministic character of the solutions is the reason for which a statistical approach was needed for a theory of turbulence to see the day. We owe this theory to Andrei Nikolaevich Kolmogorov. He published this work in 1941 in three papers (Kolmogorov, 1941a;b;c), the first being the most famous one. A rigorous treatment of Kolmogorov theory is given by Frisch (1995).

Since 1922, Richardson described turbulence by his poem:

Big whorls have little whorls,
Which feed on their velocity;
And little whorls have lesser whorls,
And so on to viscosity
(in the molecular sense).

Kinetic energy is injected through the bigger whorls, whose size L is set by the outer scale of the turbulence. The scale l at which the kinetic energy is dissipated by viscosity is called the

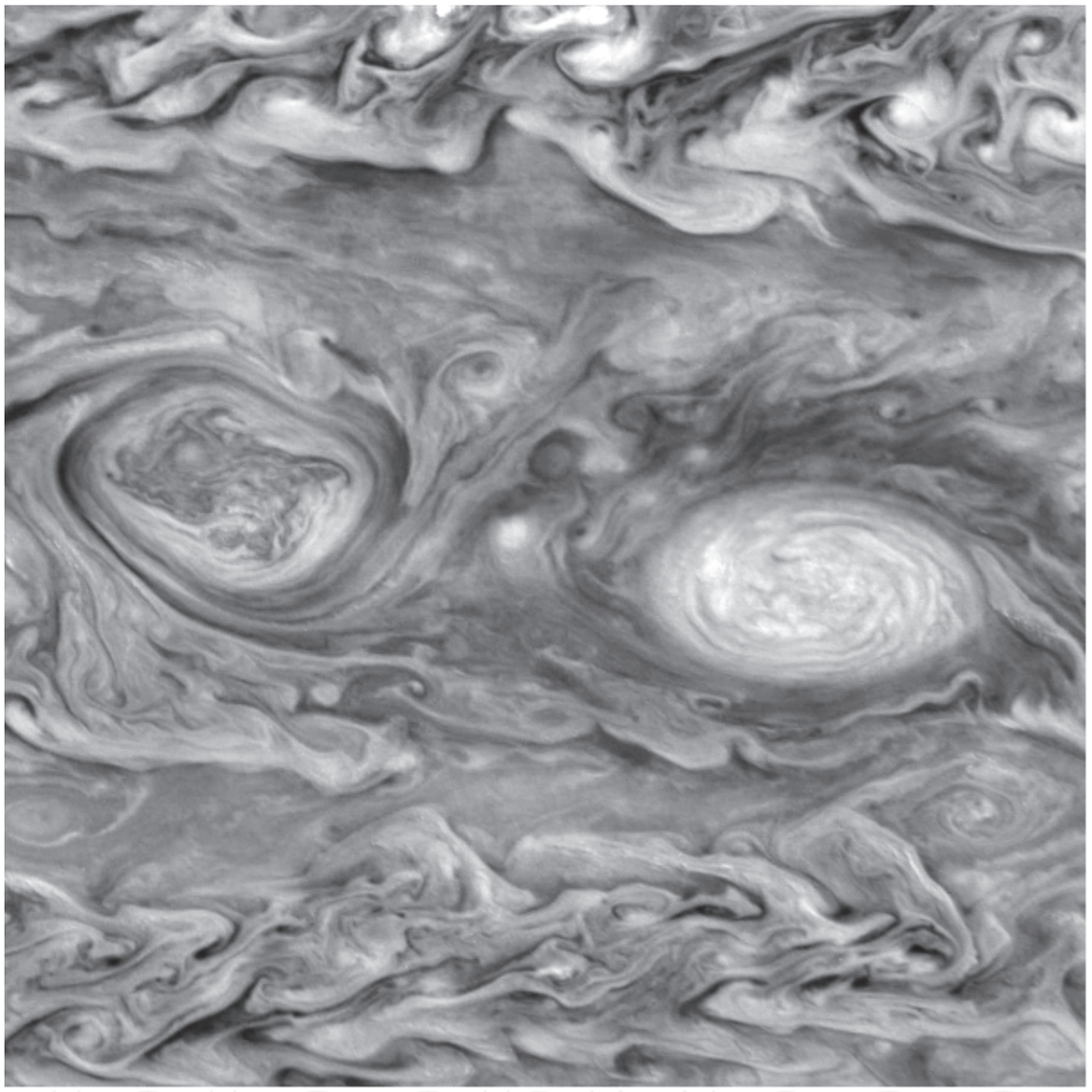

Fig. 1. Turbulence in Jupiter's atmosphere. Each of the two large eddies in the center have a dimension of 3500 km along the nort-south (up-down) direction. Image was obtained by the Galileo mission on may 7 1997. (source:
`http://photojournal.jpl.nasa.gov/animation/PIA01230`

inner scale and corresponds to the smallest turbulent elements. Kolmogorov proposed that the kinetic energy is transferred from larger to smaller eddies at a rate ϵ that is independent from the eddy spatial scale ρ. This is the so called "Kolmogorov cascade". Under this hypothesis, in the case of a completely developed turbulence and considering homogenous and isotropic three-dimensional velocity fluctuations, Kolmogorov showed that the second order structure function[1] is written as:

$$D_v(\rho) \propto \epsilon^{2/3} \rho^{2/3} \,, \tag{1}$$

[1] the second order structure function is commonly called just structure function

for scales ρ within the inertial scale defined as $l \ll \rho \ll L$. In the terrestrial atmosphere, l is of the order of a few millimeters. The outer scale L is of the order of hundreds of meters in the free atmosphere and close to the ground it is given approximately by the altitude above the ground.

2.2 Refractive index fluctuations

The perturbations of the phase of electromagnetic waves traveling through a turbulent medium like the atmosphere are due to fluctuations of the refractive index N, also called optical turbulence. In the domain of visible wavelengths, the optical turbulence is principally provoked by temperature fluctuations. In the mid infrared and radio ranges, the water vapor content is the dominant factor.

I underline that it is not the turbulent wind velocity field (dynamical turbulence) which is directly responsible of the refractive index fluctuations. Coulman et al. (1995) propose the following phenomenological description of the appearance of optical turbulence. First, dynamical turbulence needs to be triggered. For that to happen, vertical movements of air parcels have to be strong enough to break the stability imposed by the stratification in the atmosphere. In the free atmosphere this occurs when the power associated to wind shear (wind velocity gradient) exceeds that of the stratification. The quotient of those energies is represented by the mean Richardson number:

$$\mathrm{Ri} = \frac{g}{\theta} \frac{\partial \bar{\theta}/\partial z}{|\partial \bar{\mathbf{u}}/\partial z|^2} \tag{2}$$

where g is the acceleration of gravity, $\bar{\theta}$ is the mean potential temperature, $\bar{\mathbf{u}}$ is the mean wind velocity and z is the vertical coordinate. If Ri is higher than $1/4$, then the air flow is laminar. If Ri is lower than $1/4$ but positive, then the flow is turbulent and if Ri is negative then the flow is convective. When turbulence develops in a zone of the atmosphere, one expects that air at slightly different temperatures mix together, which generates optical turbulence. After some time, the temperature within that layer tends to an equilibrium and although turbulent motions of air may prevail, no optical turbulence is present. Only at the boundaries of that turbulent layer air at different temperatures may be mixing, giving birth to thin otical turbulence layers. This phenomenology would explain the relative thinness found in the optical turbulence layers (tens of meters) measured with instrumented balloons and the fact the layers tend to appear in pairs (one for each boundary of the correspoding dynamical turbulent layer). If the fluctuations of N are not substantially anisotropic within a layer, then the outer scale L_0 of the optical turbulence in that layer cannot exceed the layer thickness. Distinction must be made between the outer scale of the dynamical turbulence - which is of the order of hundreds of meters - and that of the optical turbulence L_0 which has been shown to have a median value of about 25 m at some sites (Martin et al., 1998) or even 6 m at Dome C (Ziad et al., 2008). Those measurements were carried on with the dedicated instrument called Generalized Seeing Monitor (former Grating Scale Monitor). The optical turbulence inner scale l_0 keeps the same size as l.

Based upon the theory of the temperature field micro-sctructure in a turbulent flow (Obukhov, 1949; Yaglom, 1949), Tatarski studied the turbulent fluctuations of N in his research of the propagation of waves in turbulent media, published in russian in 1959 and then translated in

english (Tatarski, 1961). He showed that the refractive index structure function has a similar expression as Eq. 1:

$$D_N(\rho) = C_{\mathrm{N}}^2 \, \rho^{2/3} \text{ , for } l_0 \ll \rho \ll L_0 \, . \tag{3}$$

The refractive index structure constant, C_{N}^2 determines the intensity of optical turbulence.

When an electromagnetic wave, coming from an astronomical object, travels across an optical-turbulence layer, it suffers phase fluctuations due to the fluctuations of N within the layer. At the exit of that layer, one can consider that the wave amplitude is not affected because the diffraction effects are negligible along a distance equal to the layer thickness. This is the approximation known as *this screen*. However, the wave reaching the ground, having gone through multiple *this screens* along the lowest 20 km of the atmosphere approximately, carries amplitude and phase perturbations. In the weak perturbation hypothesis, which is generally valid at astronomical observatories when the zenith angle does not exceed 60°, the power spectrum of the fluctuations of the complex amplitude $\Psi(\mathbf{r})$ ($\mathbf{r}$ indicating a position on the wavefront plane) can be written as

$$W_\Psi(\mathbf{f}) = W_\varphi(\mathbf{f}) + W_\chi(\mathbf{f}) \, , \tag{4}$$

where $W_\varphi(\mathbf{f})$ and $W_\chi(\mathbf{f})$ stand for the power spectra of the phase and the amplitude logarithm fluctuations, respectively, and $\mathbf{f}$ represents the spatial frequency on the wavefront plane. For a wavelength λ, the expressions of those power spectra are Roddier (1981):

$$W_\Psi(\mathbf{f}) = 0.38\lambda^{-2} f^{-11/3} \int \mathrm{d}h \; C_N^2(h) \tag{5}$$

$$W_\varphi(\mathbf{f}) = 0.38\lambda^{-2} f^{-11/3} \int \mathrm{d}h \; C_N^2(h) \cos^2\left(\pi\lambda h f^2\right) \tag{6}$$

$$W_\chi(\mathbf{f}) = 0.38\lambda^{-2} f^{-11/3} \int \mathrm{d}h \; C_N^2(h) \sin^2\left(\pi\lambda h f^2\right) \, , \tag{7}$$

which are valid for spatial frequencies within the inertial zone. All the equations given in this Chapter refer to observations made at the zenith. When observations are carried on with zenith angle z, the altitude variable h is to be replaced by $h/\cos(z)$.

Fried (1966) gave a relation analogous to Eq. 4 for the structure functions:

$$D_\Psi(\mathbf{r}) = D_\varphi(\mathbf{r}) + D_\chi(\mathbf{r}) \, , \tag{8}$$

and proposed the simple expression

$$D_\Psi(\mathbf{r}) = 6.88 \left(\frac{r}{r_0}\right)^{5/3} \, , \tag{9}$$

where r_0 is the well known Fried's parameter, given by

$$r_0 = \left[0.423 \left(\frac{2\pi}{\lambda}\right)^2 \int \mathrm{d}h \; C_N^2(h)\right]^{-3/5} \, . \tag{10}$$

This parameter defines the quality of point-source long-exposure-time images, of which the angular size is proportional to λ/r_0, for a telescope larger than r_0. Fried's parameter can be

interpreted as the size of a telescope which in a turbulence-free medium would provide the same angular resolution as that given by an infinitely large telescope with turbulence.

2.3 Stellar scintillation

The fluctuations of the wave amplitude at ground level translate into intensity fluctuations. This is responsible of stellar scintillation which is visible with the naked eye. The power spectrum $W_I(\mathbf{f})$ of the spatial fluctuations of the intensity $I(\mathbf{r})$ is written in terms of that of the amplitude logarithm as

$$W_I(\mathbf{f}) = 4W_\chi(\mathbf{f})\ . \tag{11}$$

The spatial autocovariance of scintillation produced by a turbulent layer at an altitude h, strength C_N^2 and thickness δh is given by

$$\mathcal{C}(r) = C_N^2(h)\delta h\ K(r,h), \tag{12}$$

where r stands for the modulus of the position vector $\mathbf{r}$ and $K(r,h)$ is given by the Fourier transform of the power spectrum W_I of the irradiance fluctuations (Eqs. 11 and 7). The expression for $K(r,h)$ in the case of Kolmogorov turbulence and weak perturbation approximation is (Prieur et al., 2001) :

$$K(r,h) = 0.243k^2 \int_0^\infty \mathrm{d}f\ f^{-8/3} \sin^2\left(\pi\lambda h f^2\right) J_0\left(2\pi f r\right), \tag{13}$$

where $k = 2\pi/\lambda$. Note that the scintillation variance, $\sigma_I^2 = \mathcal{C}(0)$, is proportional to $h^{5/6}$ (as can be easily deduced from Eqs. 12 and 13 by changing the integration variable to $\xi = h^{1/2}f$). Therefore as the turbulence altitude is lower, σ_I^2 decreases. In the limit, a single layer at ground level ($h = 0$) produces no scintillation. In § 3 I present a method for ground turbulence to produce detectable scintillation. It is the Generalized SCIDAR principle.

The scintillation index is defined as $\sigma_I^2/\langle I\rangle^2$, $\langle I\rangle$ being the mean intensity. Typical values for stellar scintillation index are of the order of 10% in astronomical sites at the zenith. A thorougful treatment of stellar scintillation is presented by Dravins et al. (1997a;b; 1998).

3. Generalized SCIDAR based techniques

3.1 Generalized SCIDAR

The Scintillation Detection and Ranging (SCIDAR) technique, proposed by Vernin & Roddier (1973), is aimed at the measurement of the optical-turbulence profile. The method and the physics involved have thoroughly been treated by a number of authors (Klückers et al., 1998; Prieur et al., 2001; Rocca et al., 1974; Vernin & Azouit, 1983a;b). Here I only recall the guidelines of the principle.

The SCIDAR method consists of the following: Light coming from two stars separated by an angle ρ and crossing a turbulent layer at an altitude h casts on the ground two identical scintillation patterns shifted from one another by a distance ρh. The spatial autocovariance of the compound scintillation exhibits peaks at positions $\mathbf{r} = \pm\rho h$ with an amplitude proportional to the C_N^2 value associated to that layer. The determination of the position and amplitude of those peaks leads to $C_N^2(h)$. This is the principle of the so-called Classical

SCIDAR (CS), in which the scintillation is recorded at ground level by taking images of the telescope pupil while pointing a double star. As the scintillation variance produced by a turbulent layer at an altitude h is proportional to $h^{5/6}$, the CS is blind to turbulence close to the ground, which constitutes a major disadvantage because the most intense turbulence is often located at ground level (Avila et al., 2004; Chun et al., 2009).

To circumvent this limitation, Fuchs et al. (1994) proposed to optically shift the measurement plane a distance $h_{\rm gs}$ below the pupil. For the scintillation variance to be significant, $h_{\rm gs}$ must be of the order of 1 km or larger. This is the principle of the Generalized SCIDAR (GS) which was first implemented by Avila et al. (1997). In the GS, a turbulent layer at an altitude h produces autocovariance peaks at positions $\mathbf{r} = \pm\rho(h + h_{\rm gs})$, with an amplitude proportional to $(h + h_{\rm gs})^{5/6}$. The cut of the peak centered at $\mathbf{r} = \rho(h + h_{\rm gs})$, along the direction of the double-star separation is given by

$$\mathcal{C}\left(r - \rho\left(h + h_{\rm gs}\right)\right) = C_{\rm N}^2(h)\delta h\, K\left(r - \rho\left(h + h_{\rm gs}\right), h + h_{\rm gs}\right). \tag{14}$$

In the realistic case of multiple layers, the autocovariance corresponding to each layer adds up because of the statistical independence of the scintillation produced in each layer. Hence, Eq. 14 becomes:

$$\mathcal{C}_{\rm multi}\left(r - \rho\left(h + h_{\rm gs}\right)\right) = \int_{-h_{\rm gs}}^{+\infty} {\rm d}h\, C_{\rm N}^2(h)\delta h\, K\left(r - \rho\left(h + h_{\rm gs}\right), h + h_{\rm gs}\right). \tag{15}$$

For h between $-h_{\rm gs}$ and 0, $C_{\rm N}^2(h) = 0$ because that space is virtual. To invert Eq. 15 and determine $C_{\rm N}^2(h)$, a number of methods have been used like Maximum Entropy (Avila et al., 1997), Maximum likelihood (Johnston et al., 2002; Klückers et al., 1998) or CLEAN (Avila et al., 2008; Prieur et al., 2001).

The altitude resolution or sampling interval of the turbulence profile is equal to $\Delta d/\rho$, where Δd is the minimal measurable difference of the position of two autocorrelation peaks. The natural value of Δd is the full width at half maximum L of the aucorrelation peaks: $L(h) = 0.78\sqrt{\lambda(h - h_{\rm gs})}$ (Prieur et al., 2001), where λ is the wavelength. However, Δd can be shorter than L if the inversion of Eq. 15 is performed using a method that can achieve super-resolution like Maximum Entropy or CLEAN. Both methods have been used in GS measurements (Prieur et al., 2001). Fried (1995) analized the CLEAN algorithm and its implications for super-resolution. Applying his results for GS leads to an altitude resolution of

$$\Delta h = \frac{2}{3}\frac{L}{\rho} = 0.52\frac{\sqrt{\lambda(h + h_{\rm gs})}}{\rho}. \tag{16}$$

The maximum altitude, $h_{\rm max}$ for which the $C_{\rm N}^2$ value can be retrieved is set by the altitude at which the projections of the pupil along the direction of each star cease to be overlapped, as no correlated speckles would lie on the scintillation images coming from each star. Figure 2 illustrates the basic geometrical consideration involved in the determination of $h_{\rm max}$. Note that $h_{\rm max}$ does not depend on $h_{\rm gs}$. The maximum altitude is thus given by

$$h_{\rm max} = \frac{D}{\rho}, \tag{17}$$

where D is the pupil diameter.

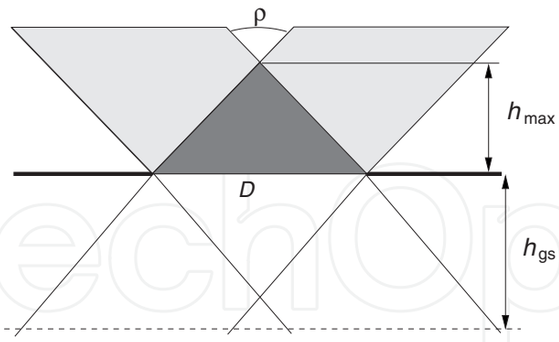

Fig. 2. Schematic for the determination of the maximum altitude h_{max} for which the C_N^2 value can be retrieved. The altitude of the analysis plane h_{gs} is represented only to make clear that this value is not involved in the calculation of h_{max}.

The procedure to estimate the scintillation autocovariance $\mathcal{C}$ is to compute the mean autocorrelation of double-star scintillation images, normalized by the autocorrelation of the mean image. In the classical SCIDAR - where images are taken at the telescope pupil - this computation leads analytically to $\mathcal{C}$ (Rocca et al., 1974). However for the GS, Johnston et al. (2002) pointed out that the result of this procedure is not equal to $\mathcal{C}$. The discrepancy is due to the shift of the out-of-focus pupil images produced by each star on the detector. Those authors analyzed this effect only for turbulence at ground level ($h = 0$) and Avila & Cuevas (2009) generalized the analysis to turbulence at any height. The effect of this misnormalization is to overestimate the C_N^2 values. The relative error is a growing function of the turbulence altitude h, the star separation ρ, the conjugation distance h_{gs} and a decreasing function of the telescope diameter D. Some configurations lead to minor modification of $C_N^2(h)$ like in Avila et al. (2011) but others provoke large discrepancies like in García-Lorenzo & Fuensalida (2011).

3.2 Low layer SCIDAR

The Low Layer SCIDAR (LOLAS) is aimed at the measurement of turbulence profiles with very high altitude-resolution but only within the first kilometer above the ground at most. The interest of such measurements resides in the need of them for constraining the design and performance estimations of adaptive optics systems dedicated to the correction of wavefront deformations induced near the ground - the so-called Ground Layer Adaptive Optics (GLAO).

LOLAS concept consists of the implementation of the GS technique on a small dedicated telescope, using a very widely separated double star. For example, for $h_{gs} = 2$ km, $h = 0$, $\lambda = 0.5$ μm, $D = 40$ cm and star separations of $180''$ and $70''$, the altitude resolution Δh equals 19 and 48 m, while the maximum sensed altitude h_{max} equals 458 and 1179 m, respectively. GS uses a larger telescope (at least 1-m diameter) and closer double stars, so that the entire altitude-range with non-negligible C_N^2 values is covered ($h_{max} \gtrsim 30$ km).

The altitude of the analysis plane, h_{gs} is set 2 km below the ground, as a result of a compromise between the increase of scintillation variance, which is proportional to $|h + h_{gs}|^{5/6}$, and the reduction of pupil diffraction effects. Indeed, pupil diffraction caused by the virtual distance between the pupil and the analysis planes provokes that Eq. 15 is only an approximation. The larger h_{gs} or the smaller the pupil diameter, the greater the error in applying Eq. 15. Numerical

simulations to estimate such effect have been performed and the pertinent corrections are applied in the inversion of Eq. 15.

The pixel size projected on the pupil, d_p, is set by the condition that the smallest scintillation speckles be sampled at the Nyquist spatial frequency or better. The typical size of those speckles is equal to $L(0)$. Taking the same values as above for h_gs and λ, yields $L(0) = 2.45$ cm. I chose $d_\mathrm{p} = 1$ cm, which indeed satisfies the Nyquist criterion $d_\mathrm{p} \leq L(0)/2$. The altitude sampling of the turbulence profiles is $\delta_h = d_p/\rho$. Note, from the two last expressions and Eq. 16, that the altitude resolution Δh and the altitude sampling δ_h are related by $\delta_h \leq (3/4)\Delta h$ for $h = 0$.

3.3 Measurement of velocity profiles

Wind-velocity profiles $\mathbf{V}(h)$ can be computed from the mean cross-correlation of images taken at times separated by a constant delay Δt. Note that the mean autocorrelation and mean cross-correlation need to be normalized by the autocorrelation of the mean image. Hereafter, I will refer to this mean-normalized cross-correlation simply as *cross-correlation*. The method is based on the following principle:

Let us assume that the turbulent structures are carried by the mean wind without deformation. This assumption is known as *Taylor hypothesis*, and is valid for short enough time intervals. In this case, the scintillation pattern produced by a layer at altitude h, where the mean horizontal wind velocity is $\mathbf{V}(h)$, moves on the analysis plane a distance $\mathbf{V}(h)\,\Delta t$ in a time Δt. If the source was a single star, the cross-correlation of images separated by a lapse Δt, would produce a correlation peak located at the point $\mathbf{r} = \mathbf{V}(h)\,\Delta t$, on the correlation map. By determining this position, one can deduce $\mathbf{V}(h)$ for that layer. As a double star is used, the contribution of the layer at altitude h in the cross-correlation consists of three correlation peaks, which we call a triplet: a central peak located at $\mathbf{r} = \mathbf{V}(h)\,\Delta t$ and two lateral peaks separated from the central one by $\pm\boldsymbol{\rho}H$, where H is the distance from the analysis plane to the given layer $H = h + h_\mathrm{gs}$ and $\boldsymbol{\rho}$ is the angular separation of the double star. The cross-correlation can be written as:

$$C_\mathrm{c}^{**}(\mathbf{r}, \Delta t) = \int_0^\infty \mathrm{d}h\, C_\mathrm{N}^2(h)\, \{\, a\, \mathcal{C}_\mathrm{c}(\mathbf{r} - \mathbf{V}(h)\Delta t, H) + b\, [\, \mathcal{C}_\mathrm{c}(\mathbf{r} - \mathbf{V}(h)\Delta t - \boldsymbol{\rho}H, H) + \mathcal{C}_\mathrm{c}(\mathbf{r} - \mathbf{V}(h)\Delta t + \boldsymbol{\rho}H, H)\,]\, \}. \tag{18}$$

$\mathcal{C}_\mathrm{c}$ is the theoretical cross-correlation of the scintillation produced by a layer at an altitude h and unit C_N^2. It differs from the theoretical autocorrelation $\mathcal{C}$ only by an eventual temporal decorrelation of the scintillation (partial failure of Taylor hypothesis) and an eventual fluctuation of $\mathbf{V}(h)$ during the integration time. The decorrelation would make $\mathcal{C}_\mathrm{c}$ smaller than $\mathcal{C}$, and the fluctuation of $\mathbf{V}(h)$ would make $\mathcal{C}_\mathrm{c}$ smaller and wider than $\mathcal{C}$ (Caccia et al., 1987). Those effects do not affect the determination of $\mathbf{V}(h)$, as the only information needed here is the position of each correlation peak. Note that $\mathcal{C}$ takes into account the spatial filtering introduced by the detector sampling. The factors a and b are given by the magnitude difference of the two stars Δm through:

$$a = \frac{1+\alpha^2}{(1+\alpha)^2} \quad \text{and} \quad b = \frac{\alpha}{(1+\alpha)^2}, \quad \text{with} \quad \alpha = 10^{-0.4\Delta m}. \tag{19}$$

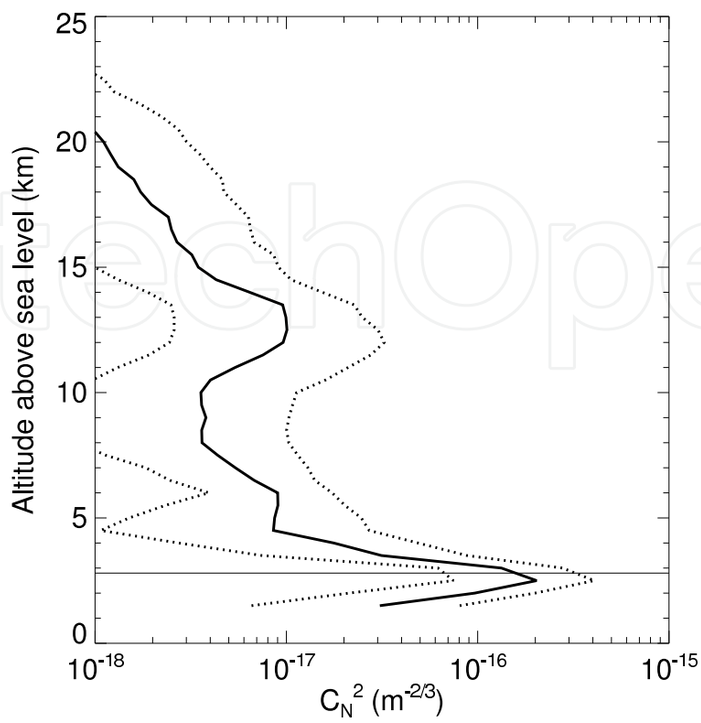

Fig. 3. Median (full line), 1st and 3rd quartiles (dashed lines) of the $C_N^2(h)$ values obtained with the GS at both telescopes, during 1997 and 2000 campaigns. The horizontal axis represents C_N^2 values, in logarithmic scale, and the vertical axis represents the altitude above sea level. The horizontal lines indicate the observatory altitude. Dome seeing has been removed.

4. Examples of turbulence and wind profiles results

4.1 $C_N^2(h)$ profiles with generalized SCIDAR

Turbulence profiles have been measured with the GS technique at many astronomical sites by a number of authors (Avila et al., 2008; Avila et al., 2004; 1998; 1997; 2001; Egner & Masciadri, 2007; Egner et al., 2007; Fuchs et al., 1998; Fuensalida et al., 2008; García-Lorenzo & Fuensalida, 2006; Kern et al., 2000; Klückers et al., 1998; Prieur et al., 2001; Tokovinin et al., 2005; Vernin et al., 2007; Wilson et al., 2003). Here I will summarize the results presented by Avila et al. (2004) which have been corrected for the normalization error by Avila et al. (2011).

Two GS observation campaigns have been carried out at the Observatorio Astronómico Nacional de San Pedro Mártir (OAN-SPM) in 1997 and 2000, respectively. The OAN-SPM , held by the Instituto de Astronomía of the Universidad Nacional Autónoma de México, is situated on the Baja California peninsula at 31^o 02′ N latitude, 115^o 29′ W longitude and at an altitude of 2800 m above sea level. It lies within the North-East part of the San Pedro Mártir (SPM) National Park, at the summit of the SPM sierra. Cruz-González et al. (2003) edited in a single volume all the site characteristics studied so far. In 1997, the GS was installed at the 1.5-m and 2.1-m telescopes (SPM1.5 and SPM2.1) for 8 and 3 nights (1997 March 23–30

and April 20–22 UT), whereas in 2000, the instrument was installed for 9 and 7 nights (May 7–15 and 16–22 UT) at SPM1.5 and SPM2.1. The number of $C_N^2(h)$ samples obtained in 1997 and 2000 are 3398 and 3016, respectively, making a total of 6414. The altitude scale of the profiles refers to altitude above sea level (2800 m at OAN-SPM). In GS data, part of the turbulence measured at the observatory altitude is produced inside the telescope dome. For site characterization, this contribution must be subtracted. In all the analysis presented here, dome turbulence has been removed using the procedure explained by Avila et al. (2004).

The median $C_N^2(h)$profile together with the first and third quartiles profiles are shown in Fig. 3. Almost all the time the most intense turbulence is located at the observatory altitude. There are marked layers centered at 6 and 12 km approximately above sea level. Although those layers appear clearly in the median profile, they are not present every night.

From a visual examination of the individual profiles, one can determine five altitude slabs that contain the predominant turbulent layers. These are]2,4],]4,9],]9,16],]16,21] and]21,25] km above sea level. In each altitude interval of the form]h_l,h_u] (where the subscripts l and u stand for "lower" and "upper" limits) and for each profile, I calculate the turbulence factor

$$J_{h_l,h_u} = \int_{h_l}^{h_u} \mathrm{d}h\, C_N^2(h), \tag{20}$$

and the correspondent seeing in arc seconds:

$$\epsilon_{h_l,h_u} = 1.08 \times 10^6 \lambda^{-1/5} J_{h_l,h_u}^{3/5}. \tag{21}$$

For the turbulence factor corresponding to the ground layer, $J_{2,4}$, the integral begins at 2 km in order to include the complete C_N^2 peak that is due to turbulence at ground level (2.8 km). Moreover, $J_{2,4}$ does not include dome turbulence. The seeing values have been calculated for $\lambda = 0.5\ \mu$m. In Fig. 4a the cumulative distribution functions of $\epsilon_{2,4}$ obtained at the SPM1.5 and the SPM2.1, calculated using the complete data set, are shown. The turbulence at ground level at the SPM1.5 is stronger than that at the SPM2.1. It is believed that this is principally due to the fact that the SPM1.5 is located at ground level, while the SPM2.1 is installed on top of a 20–m building. Moreover, the SPM2.1 building is situated at the observatory summit whereas the SPM1.5 is located at a lower altitude. The cumulative distributions of the seeing originated in the four slabs of the free atmosphere (from 4 to 25 km) are represented in Fig. 4b. The largest median seeing in the free atmosphere is encountered from 9 to 16 km, where the tropopause layer is located. Also in that slab the dynamical range of the seeing values is the largest, as can be noticed from the 1st and 3rd quartiles for example ($0\farcs11$ and $0\farcs39$). Particularly noticeable is the fact that the seeing in the tropopause can be very small as indicated by the left-hand-side tail of the cumulative distribution function of $\epsilon_{9,16}$. The turbulence at altitudes higher than 16 km is fairly weak. Finally, Figs. 4c and 4d show the cumulative distribution of the seeing produced in the free atmosphere, $\epsilon_{4,25}$, and in the whole atmosphere, $\epsilon_{2,25}$, respectively.

From each C_N^2 profile of both campaigns one value of the isoplanatic angle θ_0 (Fried, 1982) has been computed, using the following expression:

$$\theta_0 = 0.31 \frac{r_0}{h_0}, \tag{22}$$

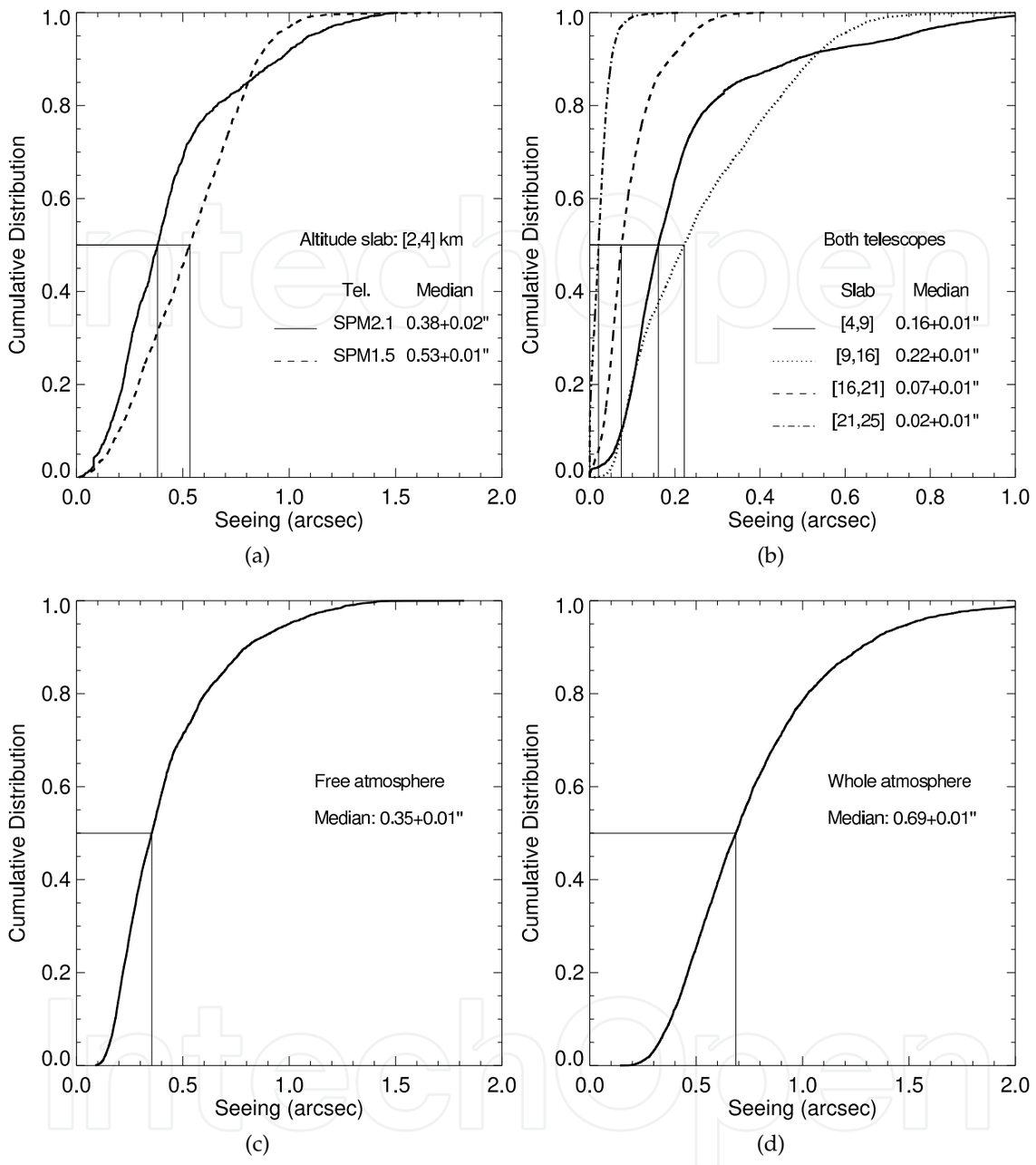

Fig. 4. Cumulative distributions of the seeing generated in different atmosphere slabs: (a)]2,4] km for the 2.1mT (full line) and the 1.5mT (dashed line) without dome seeing; (b)]4,9] km (full line),]9,16] km (dotted line),]16,21] km (dashed line),]21,25] km (dash–dotted line); (c) the free atmosphere (altitude higher than 4 km) and (d) the whole atmosphere, without dome seeing. The horizontal and vertical lines indicate the median values.

where r_0 is Fried's parameter defined in Eq. 10 and

$$h_0 = \left(\frac{\int \mathrm{d}h\, h^{5/3} C_\mathrm{N}^2(h)}{\int \mathrm{d}h\, C_\mathrm{N}^2(h)} \right)^{3/5} . \tag{23}$$

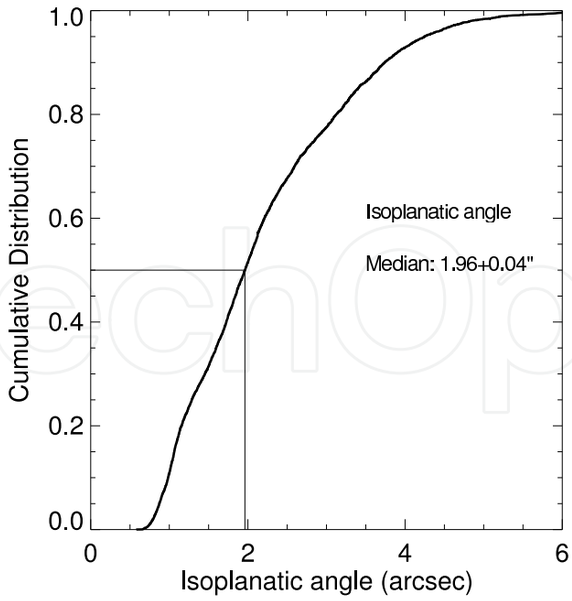

Fig. 5. Cumulative distribution of the isoplanatic angle θ_0 computed from each turbulence profile of both campaigns and both telescopes, using Eqs. 22, 10 and 23. The median value of θ_0 is 1.″96 and the 1st and 3rd quartiles are 1.″28 and 2.″85.

The cumulative distribution function of θ_0 is shown in Fig. 5. The 1st, 2nd and 3rd quartiles values are equal to 1.″28, 1.″96 and 2.″85.

4.2 $C_N^2(h)$ Profiles with low layer SCIDAR

The first results of LOLAS were obtained in September 2007 at Mauna Kea Observatory, as part of a collaboration between the Universidad Nacional Autónoma de México (UNAM), the University of Durham (UD) and the University of Hawaii (UH), under a contract with Gemini Observatory. The instrument was installed on the Coudé roof of the UH 2.2-m telescope. SLODAR and LOLAS instrument were implemented sharing the same telescope and camera. A detailed description of the campaign and results are reported by Chun et al. (2009).

To illustrate the highest altitude resolution that has so far been reached with LOLAS, Fig. 6 shows a C_N^2 profile obtained using as target a 199.″7-separation double-star. The altitude resolution in vertical direction is 11.7 m and $\Delta C_N^2 = 1.6 \times 10^{-16} \mathrm{m}^{-2/3}$. Note the ability for discerning a layer centered at 16 m from that at ground layer. Turbulence inside the telescope tube has been removed.

The quartile and 90 percentile profiles of all the C_N^2 measurements obtained with LOLAS at Mauna Kea are shown in Fg. 7. Given the consistent and very simple distribution of turbulence, the profiles were fit with an exponential form:

$$C_N^2(h)\mathrm{d} = A \exp(-h/h_{\mathrm{scale}}) + B, \tag{24}$$

where A, B and h_{scale} are constants, using a non-linear least-squares fit algorithm. The scaleheight h_{scale} of the turbulence within the ground layer increases as the integrated turbulence within the ground layer increases. The median scaleheight is 27.8 m.

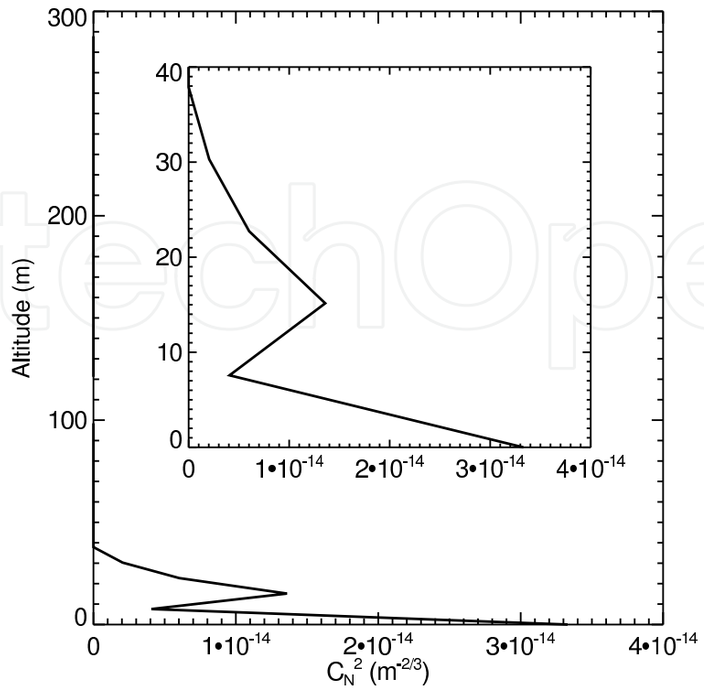

Fig. 6. Example of a turbulence profile with the highest altitude-resolution so far obtained with LOLAS. The data was taken in 2007 November 17 at 12:09 UT. The central frame shows an amplification of the profile in the low-altitude zone. The vertical axis represents altitude above the ground.

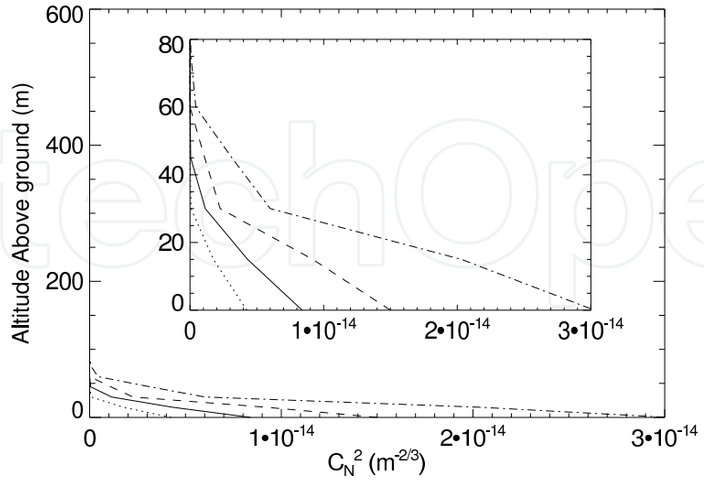

Fig. 7. Percentile profiles obtained with LOLAS at Mauna Kea. Dotter, solid, dashed and dot-dat-dashed lines represent the 25, 50,75 and 90 percentile values of C_N^2 as a function of altitude above the ground.

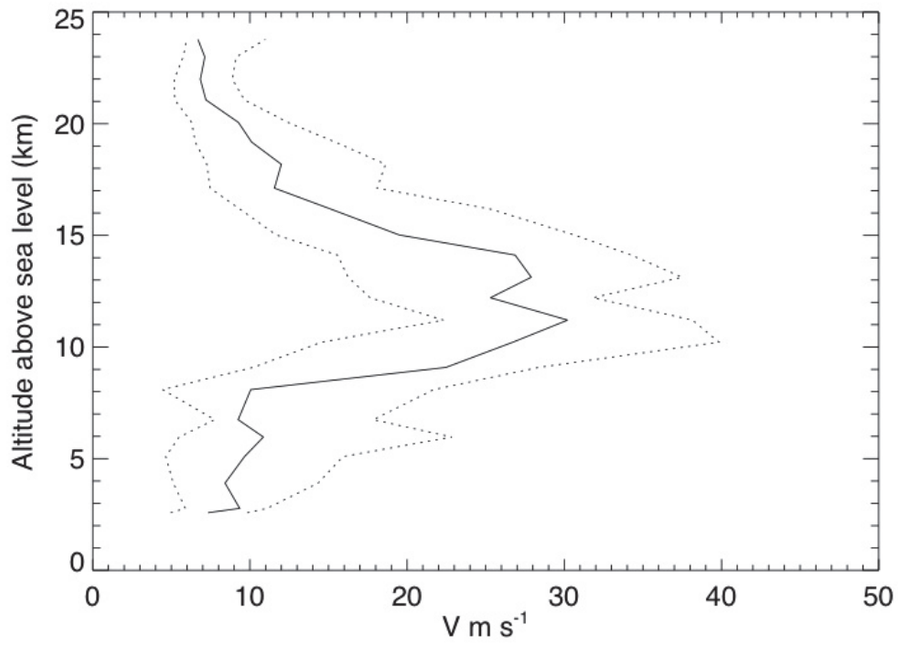

Fig. 8. Profiles of the median (solid line) and first and third quartile (dotted lines) of the wind speed.

4.3 $\mathbf{V}(h)$ profiles with generalized SCIDAR

Wind profiles were obtained at the OAN-SPM using the same data as that described in § 4.1. The median and first and third quartile values of the layer speed V as a function of height are shown in Fig. 8. It can be seen that the wind speed has similar low values within the first 4 km and above 16 km. In the jet stream zone (between 10 and 15 km), the wind speed sharply increases.

From the C_N^2 and V values of each detected layer, the coherence time τ of the wavefront deformations produced by that layer can be calculated using an expression analogous to that given by Roddier (1999):

$$\tau = 0.31 \frac{r_{0_{\text{ind}}}}{V}, \tag{25}$$

where $r_{0_{\text{ind}}}$ corresponds to the Fried's parameter that would occur if only the given layer was present:

$$r_{0_{\text{ind}}} = \left[0.423 \left(\frac{2\pi}{\lambda} \right)^2 C_N^2 \Delta h \right]^{-3/5}, \tag{26}$$

where the wavelength $\lambda = 0.5$ μm. The value of τ for a given layer sets the acceptable time delay of a deformable mirror for the mean square residual phase error of that layer, due solely to time delay, to be less than one radian. I have calculated $\tau(h)$ from each C_N^2 and $\mathbf{V}$ profiles, taking $\Delta h = 500$ m, i.e. equal to our C_N^2 profiles sampling. The median, first and third quartiles of $\tau(h)$ are shown in Fig. 9.

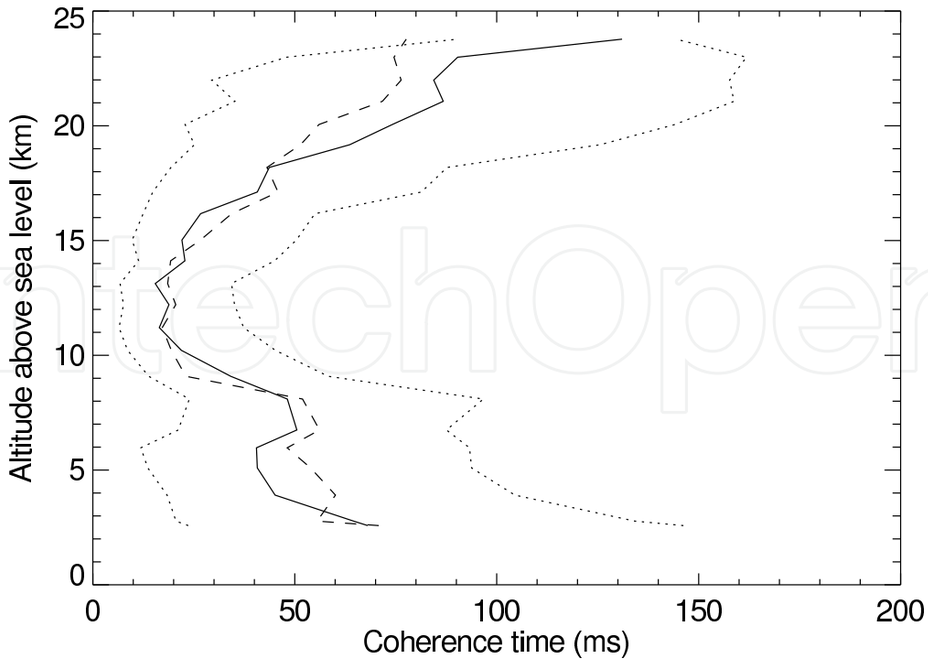

Fig. 9. Median (solid line), first and third quartiles (dotted lines) profiles of the coherence time for adaptive optics, as explained in the text (Eqs. 25 and 26). The dashed line represents the coherence time profile computed using Eq. 27.

It is interesting to note that the variation of τ with altitude, seems to be mainly governed by the variation of V. This is shown by the reasonably good agreement between the median of $\tau(h)$, and the median of the function

$$\tau_*(h) = 0.31 \frac{r_{0_{\text{med}}}}{V(h)}, \tag{27}$$

where $r_{0_{\text{med}}} = 1.8$ m, is the median value of $r_{0_{\text{ind}}}$ for all altitudes and all turbulence profiles (we remind that $r_{0_{\text{ind}}}$ is computed for 500-m slabs). The median profiles of $\tau(h)$ and $\tau_*(h)$ are shown in solid and dashed lines, respectively, in Fig. 9.

5. Summary

This chapter starts with a brief phenomenological description of the so-called optical turbulence in the atmosphere. Air flows can become turbulent when the stratification is broken due to wind shear or convection. In that case, air at different temperatures can be mixed, giving rise to a turbulent temperature field which translates into a turbulent field of the refractive index at optical wavelengths. This turbulent refractive index field is commonly known as optical turbulence. The strength of the optical turbulence is determined by the refractive index structure constant C_N^2.

After having introduced the main concepts of atmospheric optical turbulence, its effects on the propagation of optical waves and image formation are briefly presented. The spatial spectra of phase and intensity fluctuations are given for the weak perturbation approximation.

The Generalized SCIDAR (GS) technique for the measurement of the afore-mentioned vertical distributions is then presented. A recently developed application of this technique leads to the Low Layer SCIDAR (LOLAS), which is devoted to the measurement of optical turbulence profiles close to the ground with very high altitude-resolution. Those measurements are necessary for determining the expected performance and design of ground layer adaptive optics systems.

Results of GS and LOLAS measurements performed at San Pedro Mártir Observatory, Mexico and Mauna Kea Observatory, Hawaii, are finally shown, providing illustrative examples of the vertical distribution of optical turbulence in the atmosphere.

6. Acknowledgments

I am grateful to the OAN-SPM staff for their valuable support. Measurements at the OAN-SPM were carried out in the framework of a collaboration between the Instituto de Astronomía of the Universidad Nacional Autónoma de México (IA-UNAM) and the UMR 6525 Astrophysique, Université de Nice-Sophia Antipolis (France), supported by ECOS-ANUIES grant M97U01. Additional support was provided by grants J32412E and 58291 from CONACyT, IN118199, IN111403 and IN112606-2 from DGAPA-UNAM, and the TIM project (IA- UNAM). Funds for the LOLAS instrument construction and observations were provided by Gemini Observatory through con- tract number 0084699-GEM00445 entitled "Contract for Ground Layer Turbulence Monitoring Campaign on Mauna Kea".

7. References

Avila, R., Avilés, J. L., Wilson, R. W., Chun, M., Butterley, T. & Carrasco, E. (2008). LOLAS: an optical turbulence profiler in the atmospheric boundary layer with extreme altitude resolution, *Mon. Not. R. Astron. Soc.* 387: 1511–1516.

Avila, R. & Cuevas, S. (2009). On the normalization of scintillation autocovariance for generalized SCIDAR, *Optics Express* 17: 10926–+.

Avila, R., Masciadri, E., Vernin, J. & Sánchez, L. (2004). Generalized SCIDAR measurements at san pedro mártir: I. turbulence profile statistics, *Publ. Astron. Soc. Pac.* 116: 682–692.

Avila, R., Sánchez, L., Cruz-González, I., Castaño, V. M. & Carrasco, E. (2011). Recalibrated turbulence profiles at San Pedro Mártir, *Rev. Mex. Astron. Astrophys.* 47: 75–82.

Avila, R., Vernin, J. & Cuevas, S. (1998). Turbulence profiles with generalized scidar at San Pedro Mártir Observatory and isoplanatism studies, *Publ. Astron. Soc. Pac.* 110: 1106–1116.

Avila, R., Vernin, J. & Masciadri, E. (1997). Whole atmospheric-turbulence profiling with generalized scidar, *Appl. Opt.* 36(30): 7898–7905.

Avila, R., Vernin, J. & Sánchez, L. J. (2001). Atmospheric turbulence and wind profiles monitoring with generalized scidar, *Astron. Astrophys.* 369: 364.

Butterley, T., Wilson, R. W. & Sarazin, M. (2006). Determination of the profile of atmospheric optical turbulence strength from slodar data, *Mon. Not. R. Astron. Soc.* 369: 835–845.

Caccia, J. L., Azouit, M. & Vernin, J. (1987). Wind and C_n^2 profiling by single-star scintillation analysis, *Appl. Opt.* 26(7): 1288–1294.

Chun, M., Wilson, R., Avila, R., Butterley, T., Aviles, J.-L., Wier, D. & Benigni, S. (2009). Mauna Kea ground-layer characterization campaign, *Mon. Not. R. Astron. Soc.* 394: 1121–1130.

Coulman, C. E., Vernin, J. & Fuchs, A. (1995). Optical seeing-mechanism of formation of thin turbulent laminae in the atmosphere, *Appl. Opt.* 34: 5461–5474.

Cruz-González, I., Avila, R. & Tapia, M. (2003). *San Pedro Mártir: Astronomical Site Evaluation*, Vol. 19, Revista Mexicana de Astronomía y Astrofísica (serie de conferencias), Instituto de Astronomía, UNAM, México.

Dravins, D., Lindegren, L., Mezey, E. & Young, A. T. (1997a). Atmospheric Intensity Scintillation of Stars, I. Statistical Distributions and Temporal Properties, *Publ. Astron. Soc. Pac.* 109: 173–207.

Dravins, D., Lindegren, L., Mezey, E. & Young, A. T. (1997b). Atmospheric Intensity Scintillation of Stars. II. Dependence on Optical Wavelength, *Publ. Astron. Soc. Pac.* 109: 725–737.

Dravins, D., Lindegren, L., Mezey, E. & Young, A. T. (1998). Atmospheric Intensity Scintillation of Stars. III. Effects for Different Telescope Apertures, *Publ. Astron. Soc. Pac.* 110: 610–633.

Egner, S. E. & Masciadri, E. (2007). A g-scidar for ground-layer turbulence measurements at high vertical resolution, *Publ. Astron. Soc. Pac.* 119: 1441–1448.

Egner, S. E., Masciadri, E. & McKenna, D. (2007). Generalized SCIDAR Measurements at Mount Graham, *Publ. Astron. Soc. Pac.* 119: 669–686.

Fried, D. (1982). Anisoplanetism in adaptive optics, *J. Opt. Soc. Am. A* 72(1): 52–61.

Fried, D. L. (1966). Optical resolution through a randomly inhomogeneous medium for very long and very short exposures, *J. Opt. Soc. Am. A* 56(10): 1372–1379.

Fried, D. L. (1995). Analysis of the clean algorithm and implications for superresolution, *J. opt. Soc. Am. A* 12(5): 853–860.

Frisch, U. (1995). *The legacy of A. N. Kolmogorov*, Cambridge University Press, UK.

Fuchs, A., Tallon, M. & Vernin, J. (1994). Folding of the vertical atmospheric turbulence profile using an optical technique of movable observing plane, *in* W. A. Flood & W. B. Miller (eds), *Atmospheric Propagation and Remote Sensing III*, Vol. 2222, pp. 682–692.

Fuchs, A., Tallon, M. & Vernin, J. (1998). Focussiong on a turbulent layer: Principle of the generalized SCIDAR, *Publ. Astron. Soc. Pac.* 110: 86–91.

Fuensalida, J. J., García-Lorenzo, B. & Hoegemann, C. (2008). Correction of the dome seeing contribution from generalized-SCIDAR data using evenness properties with Fourier analysis, *Mon. Not. R. Astron. Soc.* 389: 731–740.

García-Lorenzo, B. & Fuensalida, J. J. (2006). Processing of turbulent-layer wind speed with Generalized SCIDAR through wavelet analysis, *Mon. Not. R. Astron. Soc.* 372: 1483–1495.

García-Lorenzo, B. & Fuensalida, J. J. (2011). Atmospheric optical turbulence at the Roque de los Muchachos Observatory: data base and recalibration of the generalized SCIDAR data, *Mon. Not. R. Astron. Soc.* pp. 1124–+.

Johnston, R. A., Dainty, C., Wooder, N. J. & Lane, R. G. (2002). Generalized scintillation detection and ranging results obtained by use of a modified inversion technique, *Appl. Opt.* 41(32): 6768–6772.

Kern, B., Laurence, T. A., Martin, C. & Dimotakis, P. E. (2000). Temporal coherence of individual turbulent patterns in atmospheric seeing, *Appl. Opt.* 39: 4879–4885.

Klückers, V. A., Wooder, N. J., Nicholls, T. W., Adcock, M. J., Munro, I. & Dainty, J. C. (1998). Profiling of atmospheric turbulence strength and velocity using a generalised SCIDAR technique, *Astron. Astrophys. Suppl. Ser.* 130: 141–155.

Kolmogorov, A. N. (1941a). Dissipation of energy in local isotropic turbulence, *Dokl. Akad. Nauk. SSSR* 32: 16.

Kolmogorov, A. N. (1941b). The local structure of turbulence in incompressible fluids with very high reynolds numbers, *Dokl. Akad. Nauk. SSSR* 30: 9.

Kolmogorov, A. N. (1941c). On degeneration (decay) of isotropic turbulence in an incompressible viscous liquid, *Dokl. Akad. Nauk. SSSR* 31: 538.

Lesieur, M. (1994). *La Turbulence*, Presses Universitaires de Grenoble, Grenoble.

Martin, F., Tokovinin, A., Ziad, A., Conan, R., Borgnino, J., Avila, R., Agabi, A. & Sarazin, M. (1998). First statistical data on wavefront outer scale at La Silla Observatory from the GSM instrument, *Astron. Astrophys.* 336: L49–L52.

Obukhov, A. M. (1949). Structure of the temperature field in a turbulent flow, *Izv. Akad. Nauk. SSSR, Ser Geograf. Geofiz.* 13: 58–69.

Prieur, J.-L., Daigne, G. & Avila, R. (2001). Scidar measurements at pic du midi, *Astron. Astrophys.* 371: 366–377.

Rocca, A., Roddier, F. & Vernin, J. (1974). Detection of atmospheric turbulent layers by spatiotemporal and spatioangular correlation measurements of stellar-light scintillation., *Journal of the Optical Society of America (1917-1983)* 64: 1000–1004.

Roddier, F. (1981). The effect of atmospheric turbulence in optical astronomy, *Progress in Optics* XIX: 281–376.

Roddier, F. (1999). *Adaptive optics in astronomy*, Cambridge University Press, United Kingdom.

Rousset, G. (1994). Wavefront Sensing, *in* D. M. Alloin & J. M. Mariotti (ed.), *NATO ASIC Proc. 423: Adaptive Optics for Astronomy*, pp. 115–+.

Tatarski, V. I. (1961). *Wave Propagation in a Turbulent Medium*, Dover Publications, Inc., New York.

Tokovinin, A., Vernin, J., Ziad, A. & Chun, M. (2005). Optical Turbulence Profiles at Mauna Kea Measured by MASS and SCIDAR, *Publ. Astron. Soc. Pac.* 117: 395–400.

Vernin, J. & Azouit, M. (1983a). Traitement d'image adapté au speckle atmosphérique. I-formation du speckle en atmosphère turbulente. propriétés statistiques, *Journal of Optics (Paris)* 14: 5–9.

Vernin, J. & Azouit, M. (1983b). Traitement d'image adapté au speckle atmosphérique. II-analyse multidimensionnelle appliquée au diagnostic à distance de la turbulence, *Journal of Optics (Paris)* 14: 131–142.

Vernin, J. & Roddier, F. (1973). Experimental determination of two-dimensional spatiotemporal power spectra of stellar light scintillation. evidence for a multilayer structure of the air turbulence in the upper troposphere, *J. opt. Soc. Am. A* 63: 270–273.

Vernin, J., Trinquet, H., Jumper, G., Murphy, E. & Ratkowski, A. (2007). OHP02 gravity wave campaign in relation to optical turbulence, *Environmental Fluid Mechanics* 7: 371–+.

Wilson, R., Butterley, T., Sarazin, M., Lombardi, G., Chun, M., Benigni, S., Weir, D., Avila, R. & Aviles, J.-L. (2008). SLODAR turbulence monitors for real-time support of astronomical adaptive optics, *Society of Photo-Optical Instrumentation Engineers (SPIE) Conference Series*, Vol. 7015 of *Society of Photo-Optical Instrumentation Engineers (SPIE) Conference Series*.

Wilson, R. W., Bate, J., Guerra, J. C., Sarazin, M. & Saunter, C. (2004). Development of a portable slodar turbulence profiler, *in* D. Bonnaccini, B. Ellerbroek & R. Raggazzoni (eds), *Advancements in Adaptive Optics*, Vol. 5490, SPIE, pp. 758–765.

Wilson, R. W., Wooder, N. J., Rigal, F. & Dainty, J. C. (2003). Estimation of anisoplanatism in adaptive optics by generalized SCIDAR profiling, *Mon. Not. R. Astron. Soc.* 339: 491–494.

Yaglom, A. (1949). On the local structure of the temperature field in a turbulent flow, *IDokl. Akad. Nauk. SSSR* 69: 743–746.

Ziad, A., Aristidi, E., Agabi, A., Borgnino, J., Martin, F. & Fossat, E. (2008). First statistics of the turbulence outer scale at Dome C, *Astron. Astrophys.* 491: 917–921.

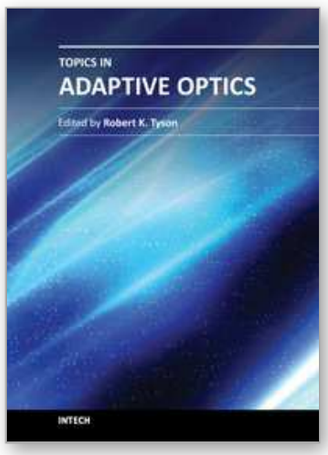

Topics in Adaptive Optics
Edited by Dr. Bob Tyson

ISBN 978-953-307-949-3
Hard cover, 254 pages
Publisher InTech
Published online 20, January, 2012
Published in print edition January, 2012

Advances in adaptive optics technology and applications move forward at a rapid pace. The basic idea of wavefront compensation in real-time has been around since the mid 1970s. The first widely used application of adaptive optics was for compensating atmospheric turbulence effects in astronomical imaging and laser beam propagation. While some topics have been researched and reported for years, even decades, new applications and advances in the supporting technologies occur almost daily. This book brings together 11 original chapters related to adaptive optics, written by an international group of invited authors. Topics include atmospheric turbulence characterization, astronomy with large telescopes, image post-processing, high power laser distortion compensation, adaptive optics and the human eye, wavefront sensors, and deformable mirrors.

InTech Europe
University Campus STeP Ri
Slavka Krautzeka 83/A
51000 Rijeka, Croatia
Phone: +385 (51) 770 447
Fax: +385 (51) 686 166
www.intechopen.com

InTech China
Unit 405, Office Block, Hotel Equatorial Shanghai
No.65, Yan An Road (West), Shanghai, 200040, China
中国上海市延安西路65号上海国际贵都大饭店办公楼405单元
Phone: +86-21-62489820
Fax: +86-21-62489821

IntechOpen